6632 *Chem. Mater.* **2010,** *22,* 6632–6640
DOI:10.1021/cm102601v

CHEMISTRY OF MATERIALS
Article

Synthesis and Stability of Tagged UiO-66 Zr-MOFs

Mathivathani Kandiah,[†] Merete Hellner Nilsen,[†] Sandro Usseglio,[†] Søren Jakobsen,[†] Unni Olsbye,[†] Mats Tilset,[†] Cherif Larabi,[‡] Elsje Alessandra Quadrelli,[‡] Francesca Bonino,[§] and Karl Petter Lillerud*[,†]

[†]*Department of Chemistry, University of Oslo, P.O. Box 1033, N-0315 Oslo, Norway,* [‡]*Université de Lyon, LCOMS, UMR 5265 C2P2 CPE-UCBL1-CNRS Bâtiment 308 ; 43 Boulevard du 11 Novembre 1918; F-69616, Villeurbanne, France, and* [§]*Department of Chemistry IFM & NIS Centre of Excellence, University of Torino, Via Quarello 11, I-10125 Torino, Italy*

Received September 10, 2010. Revised Manuscript Received November 2, 2010

The development in the field MOF materials is moving from the discovery of new structures toward applications of the most promising materials. In most cases, specialized applications require incorporation of functional chemical groups. This work is a systematic investigation of the effect that simple substituents attached to the aromatic linker have on the stability and property to the parent MOF. A family of isoreticular MOFs, based on the UiO-66 structure was obtained from the three different linker ligands H_2N-H_2BDC, O_2N-H_2BDC, and $Br-H_2BDC$. The physicochemical and chemical investigation of these materials demonstrate that this class of MOFs retains high thermal and chemical stabilities, even with functional groups present at the linker units. The results demonstrate the possibility of incorporating active functional groups into the UiO-66 structure almost without losing its exceptionally high thermal and chemical stability. It has been established that the functional groups, at least in the amino functionalized UiO-66 sample, are chemically available as evidenced by the H/D exchange experiment, making the tagged UiO series MOFs very interesting for further studies within the field of catalysis.

Introduction

An exceptional challenge in MOF synthesis is to modify chemical composition, functionality, and molecular dimensions systematically without altering the original topology.[1] Widespread interest in the aforementioned aim has resulted in a rational, designed approach in the preparation of MOFs, where the choice of metal ion and ligand can be judiciously selected.[2−7] Although the ability to incorporate different metal centers into MOFs has improved,[8−10] the introduction of ligands containing functional groups into the MOF is still a challenging issue because of the reactivity of such groups under preparative conditions.[11] In this regard, to design a structure with desired properties, the starting building blocks should satisfy two particular requirements: (i) contain the relevant features necessary to build the skeleton and (ii) have different functionalities and dimensions that can be adopted under similar synthesis conditions to produce structures with the same topology.

During the last 10 years, impressive progress has been made and this approach has been advanced to a point that allows the design of porous structures in which pore sizes and functionalities can be varied systematically.[1−6,8−13] These types of porous materials are currently attracting considerable attention for their possible use in applications such as gas storage,[14−19] catalysis,[20−26] separations,[27−33] drug delivery,[34−38] and sensors.[39−43]

*To whom correspondence should be addressed. E-mail: k.p.lillerud@kjemi.uio.no.

(1) Eddaoudi, M.; Kim, J.; Rosi, N.; Vodak, D.; Wachter, J.; O'Keeffe, M.; Yaghi, O. M. *Science* **2002**, *295*, 469–472.
(2) Kitaura, R.; Iwahori, F.; Matsuda, R.; Kitagawa, S.; Kubota, Y.; Takata, M.; Kobayashi, T. C. *Inorg. Chem.* **2004**, *43*, 6522–6524.
(3) Custelcean, R.; Gorbunova, M. G. *J. Am. Chem. Soc.* **2005**, *127*, 16362–16363.
(4) Kitagawa, S.; Noro, S.; Nakamura, T. *Chem. Commun.* **2006**, 701–707.
(5) Halper, S. R.; Do, L.; Stork, J. R.; Cohen, S. M. *J. Am. Chem. Soc.* **2006**, *128*, 15255–15268.
(6) Kawano, M.; Kawamichi, T.; Haneda, T.; Kojima, T.; Fujita, M. *J. Am. Chem. Soc.* **2007**, *129*, 15418–15419.
(7) Rao, C. N. R.; Natarajan, S.; Vaidhyanathan, R. *Angew. Chem., Int. Ed.* **2004**, *43*, 1466–1496.
(8) Ma, S. Q.; Zhou, H. C. *J. Am. Chem. Soc.* **2006**, *128*, 11734–11735.
(9) Forster, P. M.; Eckert, J.; Heiken, B. D.; Parise, J. B.; Yoon, J. W.; Jhung, S. H.; Chang, J. S.; Cheetham, A. K. *J. Am. Chem. Soc.* **2006**, *128*, 16846–16850.
(10) Dinca, M.; Yu, A. F.; Long, J. R. *J. Am. Chem. Soc.* **2006**, *128*, 8904–8913.
(11) Du, M.; Zhao, X. J.; Guo, H. H. *Inorg. Chem. Commun.* **2005**, *8*, 1–5.
(12) Papaefstathiou, G. S.; MacGillivray, L. R. *Coord. Chem. Rev.* **2003**, *246*, 169–184.
(13) Deng, H. X.; Doonan, C. J.; Furukawa, H.; Ferreira, R. B.; Towne, J.; Knobler, C. B.; Wang, B.; Yaghi, O. M. *Science* **2010**, *327*, 846–850.
(14) Thomas, K. M. *Catal. Today* **2007**, *120*, 389–398.
(15) Czaja, A. U.; Trukhan, N.; Muller, U. *Chem. Soc. Rev.* **2009**, *38*, 1284–1293.
(16) Greathouse, J. A.; Kinnibrugh, T. L.; Allendorf, M. D. *Ind. Eng. Chem. Res.* **2009**, *48*, 3425–3431.
(17) Kanoo, P.; Gurunatha, K. L.; Maji, T. K. *J. Mater. Chem.* **2010**, *20*, 1322–1331.
(18) Lin, X.; Jia, J. H.; Zhao, X. B.; Thomas, K. M.; Blake, A. J.; Walker, G. S.; Champness, N. R.; Hubberstey, P.; Schroder, M. *Angew. Chem., Int. Ed.* **2006**, *45*, 7358–7364.
(19) Rowsell, J. L. C.; Spencer, E. C.; Eckert, J.; Howard, J. A. K.; Yaghi, O. M. *Science* **2005**, *309*, 1350–1354.
(20) Wu, C. D.; Hu, A.; Zhang, L.; Lin, W. B. *J. Am. Chem. Soc.* **2005**, *127*, 8940–8941.
(21) Xamena, F.; Abad, A.; Corma, A.; Garcia, H. *J. Catal.* **2007**, *250*, 294–298.

 Published on Web 12/03/2010 © 2010 American Chemical Society

Additionally, one of the main weaknesses of MOF materials may be ascribed to their rather low thermal, hydrothermal, and chemical stabilities when compared with zeolites, a fact that may undoubtedly limit their use in large scale industrial applications. In this regard, rather limited data have been reported in the scientific literature up to now.[44−47] However, we recently presented a first generation of a zirconium-based MOF (UiO-66) characterized by very high surface area and with an unprecedented thermal stability. This material results by connecting together hexanuclear zirconium clusters with a simple, commercially available bridging ligand 1,4-benzenedicarboxylate (BDC), furnishing a robust, 3-dimensional porous structure, I^0O^3 according to the classification by T. Cheetham et al.[48] The high thermal stability has been attributed to the combination of strong Zr−O bonds and on the ability of the inner Zr_6 cluster to rearrange reversibly upon dehydroxylation or rehydratation of μ_3-OH groups, without detrimental effects on the stabilities of the connecting dicarboxylate bridges. The UiO-66 has a decomposition temperature above 500 °C and is quite resistant to many chemicals, and it remains crystalline even after exposure to high external pressures.[49]

Scheme 1. Linkers Used for Synthesizing Tagged MOFs

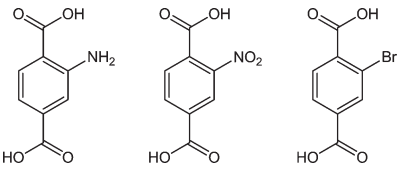

Our present goal is to assess how functionalization of BDC independently contributes to modify the chemical and physical properties of UiO-66. Herein, we report a systematic assembly of a series of frameworks that have structures based on the skeleton of UiO-66, wherein the pore functionality and size have been altered without changing the original topology. We have pursued the assembly of extended structures of the Zr-based MOF UiO-66 with three different commercially available ligands: 2-amino-benzenedicarboxylic acid (H_2N-H_2BDC), 2-nitro-benzenedicarboxylic acid (O_2N-H_2BDC), and 2-bromo-benzenedicarboxylic acid ($Br-H_2BDC$) (Scheme 1).

The synthesis of the three new functionalized MOFs UiO-66-NH_2 (**1**), UiO-66-NO_2 (**2**), and UiO-66-Br (**3**) was initiated by determining the reaction conditions necessary to produce MOFs with the same topology of the parent UiO-66. These conditions differ slightly with respect to the one previously adopted. The presence of functionality in the resulting MOFs was probed by FTIR. Thermal and structural stability of the modified MOFs were examined using powder X-ray diffraction analysis (PXRD) and thermogravimetric analysis (TGA). Langmuir surface areas were also determined using N_2 isotherms at 77 K to examine the porosity of the functionalized materials. Some changes in the surface area because of the presence of additional functionality on the BDC ligand were revealed. More importantly, considerable alteration of the chemical resistance toward strong acid and base media and on the thermal stability was noticed to occur as a consequence of the functionalization.

Experimental Methods

All chemicals were obtained commercially (Aldrich) and used without further purification.

Preparation of UiO-66-NH_2 (1), UiO-66-NO_2 (2), and UiO-66-Br (3). A standard upscaled synthesis of UiO-66-NH_2 (**1**) was performed by dissolving $ZrCl_4$ (1.50 g, 6.4 mmol) and 2-amino-1,4-benzenedicarboxylic acid (H_2N-H_2BDC) (1.56 g, 6.4 mmol) in DMF (180 mL) at room temperature in a volumetric flask. The resulting mixture was placed in a preheated oven at 80 °C for 12 h and then held at 100 °C for 24 h. After the solution was cooled to room temperature in air, the resulting solid was filtered and repeatedly washed with absolute ethanol for 3 days while heated at 60 °C in a water bath. The resulting yellow powder was filtered, transferred to a Schlenk flask, and dried under vacuum at ambient temperature.

(22) Corma, A.; GarciÌa, H.; LlabreÌs i Xamena, F. X. *Chem. Rev.* **2010**, *110*, 4606–4655.
(23) Jiang, D. M.; Mallat, T.; Meier, D. M.; Urakawa, A.; Baiker, A. *J. Catal.* **2010**, *270*, 26–33.
(24) Li, Z. Y.; Zhu, G. S.; Lu, G. Q.; Qiu, S. L.; Yao, X. D. *J. Am. Chem. Soc.* **2010**, *132*, 1490–1491.
(25) Ohara, K.; Kawano, M.; Inokuma, Y.; Fujita, M. *J. Am. Chem. Soc.* **2010**, *132*, 30–31.
(26) Pan, Y. Y.; Yuan, B. Z.; Li, Y. W.; He, D. H. *Chem. Commun.* **2010**, *46*, 2280–2282.
(27) Alaerts, L.; Maes, M.; Giebeler, L.; Jacobs, P. A.; Martens, J. A.; Denayer, J. F. M.; Kirschhock, C. E. A.; De Vos, D. E. *J. Am. Chem. Soc.* **2008**, *130*, 14170–14178.
(28) Wang, S. Y.; Yang, Q. Y.; Zhong, C. L. *Sep. Purif. Technol.* **2008**, *60*, 30–35.
(29) Couck, S.; Denayer, J. F. M.; Baron, G. V.; Remy, T.; Gascon, J.; Kapteijn, F. *J. Am. Chem. Soc.* **2009**, *131*, 6326–6327.
(30) Finsy, V.; Ma, L.; Alaerts, L.; De Vos, D. E.; Baron, G. V.; Denayer, J. F. M. *Microporous Mesoporous Mater.* **2009**, *120*, 221–227.
(31) Keskin, S.; Sholl, D. S. *Langmuir* **2009**, *25*, 11786–11795.
(32) Li, J. R.; Kuppler, R. J.; Zhou, H. C. *Chem. Soc. Rev.* **2009**, *38*, 1477–1504.
(33) Adams, R.; Carson, C.; Ward, J.; Tannenbaum, R.; Koros, W. *Microporous Mesoporous Mater.* **2010**, *131*, 13–20.
(34) Cohen, S. M. *Curr. Opin. Chem. Biol.* **2007**, *11*, 115–120.
(35) Rieter, W. J.; Taylor, K. M. L.; Lin, W. B. *J. Am. Chem. Soc.* **2007**, *129*, 9852–9853.
(36) Horcajada, P.; Serre, C.; Maurin, G.; Ramsahye, N. A.; Balas, F.; Vallet-Regi, M.; Sebban, M.; Taulelle, F.; Ferey, G. *J. Am. Chem. Soc.* **2008**, *130*, 6774–6780.
(37) Taylor-Pashow, K. M. L.; Della Rocca, J.; Xie, Z. G.; Tran, S.; Lin, W. B. *J. Am. Chem. Soc.* **2009**, *131*, 14261–14263.
(38) Horcajada, P.; Chalati, T.; Serre, C.; Gillet, B.; Sebrie, C.; Baati, T.; Eubank, J. F.; Heurtaux, D.; Clayette, P.; Kreuz, C.; Chang, J. S.; Hwang, Y. K.; Marsaud, V.; Bories, P. N.; Cynober, L.; Gil, S.; Ferey, G.; Couvreur, P.; Gref, R. *Nat. Mater.* **2010**, *9*, 172–178.
(39) Wong, K. L.; Law, G. L.; Yang, Y. Y.; Wong, W. T. *Adv. Mater.* **2006**, *18*, 1051–1054.
(40) Chen, B. L.; Yang, Y.; Zapata, F.; Lin, G. N.; Qian, G. D.; Lobkovsky, E. B. *Adv. Mater.* **2007**, *19*, 1693–1696.
(41) Achmann, S.; Hagen, G.; Kita, J.; Malkowsky, I. M.; Kiener, C.; Moos, R. *Sensors* **2009**, *9*, 1574–1589.
(42) Zou, X. Q.; Zhu, G. S.; Hewitt, I. J.; Sun, F. X.; Qiu, S. L. *Dalton Trans.* **2009**, 3009–3013.
(43) Stylianou, K. C.; Heck, R.; Chong, S. Y.; Bacsa, J.; Jones, J. T. A.; Khimyak, Y. Z.; Bradshaw, D.; Rosseinsky, M. J. *J. Am. Chem. Soc.* **2010**, *132*, 4119–4130.
(44) Ma, S. Q.; Wang, X. S.; Yuan, D. Q.; Zhou, H. C. *Angew. Chem., Int. Ed.* **2008**, *47*, 4130–4133.
(45) Han, L.; Zhou, Y.; Wang, X. T.; Li, X.; Tong, M. L. *J. Mol. Struct.* **2009**, *923*, 24–27.
(46) Kleist, W.; Maciejewski, M.; Baiker, A. *Thermochim. Acta* **2010**, *499*, 71–78.
(47) Marx, S.; Kleist, W.; Huang, J.; Maciejewski, M.; Baiker, A. *Dalton Trans.* **2010**, *39*, 3795–3798.
(48) Cheetham, A. K.; Rao, C. N. R.; Feller, R. K. *Chem. Commun.* **2006**, 4780–4795.
(49) Cavka, J. H.; Jakobsen, S.; Olsbye, U.; Guillou, N.; Lamberti, C.; Bordiga, S.; Lillerud, K. P. *J. Am. Chem. Soc.* **2008**, *130*, 13850–13851.

UiO-66-NO_2 (**2**) and UiO-66-Br (**3**) MOFs were synthesized analogously by replacing H_2N-H_2BDC with the equivalent molar amounts of O_2N-H_2BDC and $Br-H_2BDC$, respectively.

PXRD Analysis. Approximately 3 mg of UiO-66-NH_2 and modified samples were soaked in ethanol dispersed and dried as a thin layer on a glass plate before the PXRD measurements. PXRD data were collected at ambient atmosphere and temperature on a Bruker D5000 instrument with monochromatic Cu Kα_1 radiation ($\lambda = 1.540$ Å) operated in Bragg−Bretano geometry.

Surface Area Analysis. Specific surface areas were determined from nitrogen adsorption/desorption isotherms and were performed on a BEL SORP MINI system (BEL Japan, Inc.). Prior to the surface area analysis, the samples were activated in vacuum at 80 °C for 1 h and then the temperature was raised to 150 °C for 2 h.

IR Spectroscopy Analysis. The IR experiments were performed in transmission mode on a FTIR Bruker VERTEX 80 spectrometer equipped with two detectors: a cryogenic MCT detector (spectral range 4000−600 cm^{-1}) for UiO-66-NO_2 (**2**) and UiO-66-NH_2 (**1**) and a DTGS detector (spectral range 4000−400 cm^{-1}) for UiO-66-Br (**3**). The MOF under study was analyzed in the form of a thin film deposited on a silicon wafer. The thin film was prepared from an ethanol suspension of the samples. Solvent removal spectra were obtained by introducing the silicon wafer in a quartz cell that allowed "in situ" spectrum collection in a controlled atmosphere, and the sample was degassed at 373 K under dynamic vacuum (residual pressure $<10^{-2}$ Pa) for 30 min. Functionalized linker spectra were recorded by diluting the pure compound with KBr powder and pressing the mixture into a pellet form.

Raman Spectroscopy. Raman spectra were recorded on a Renishaw inVia Raman microscope spectrometer. A diode laser emitting at 785 nm was used; only 5% of the total laser power was admitted to the spectrometer. Photons scattered by the sample were dispersed by a 1200 lines/mm grating monochromator and were simultaneously collected on a CCD camera; the collection optic was set at 50× objective. The spectral collection setup of 50 acquisitions, each of 10 s duration, was adopted. The samples were prepared as powders.

Thermal Analysis. Thermogravimetric analysis (TGA) and temperature programmed adsorption/desorption (TPA/TPD) were carried out in flowing nitrogen (13 mL/min) and oxygen (3 mL/min) atmosphere using a Rheometric Scientific STA 1500 instrument with an adapted gas supply system. The TG analyses were performed with parallel online mass spectrometric (MS) analysis. The MS data were recorded with a Pfeiffer OmniStar GSD 300 O quadrupole equipped with an electron multiplier detector. The gas for MS analysis was collected with a heated steel capillary ending inside the reaction chamber 3 mm above the sample. The approximate sample weight was 10 mg in all experiments and the heating rate in TG experiments was 5 °C/min.

Temperature-Resolved PXRD. The thermal decomposition of the as-synthesized tagged UiO-66 materials in air were monitored by powder X-ray diffraction. The diffractograms were recorded on a Siemens D5000 instrument in focusing transmission geometry using Cu Kα_1 radiation. The sample was packed in a capillary (quartz, 0.7 mm) and mounted in a goniometer which was placed in a flow of hot air. Diffractograms ($2\theta = 3-25°$) were collected at several temperatures until structural decomposistion was observed. The temperature was changed in steps after the recording of a complete diffraction pattern. Two temperature increments were chosen: 50 °C in the range 100−250 and 20 °C in the range 250−410 °C.

Chemical Stability. The stability of MOF samples toward water, acid and base for UiO-66 and the three tagged materials were studied by treating the as-synthesized materials (0.2 g) with solutions (20 mL) of water, 1.0 M HCl, and 1.0 M NaOH, respectively, for 2 h at room temperature. After the treatment, the solids were filtered and dried before the XRD analyses were performed.

Results and Discussion

In a previous study, the Zr-based MOF UiO-66 was obtained via solvothermal synthesis from a DMF solution of $ZrCl_4$ and H_2BDC. The resulting mixture was sealed in an autoclave and placed in a preheated oven at 120 °C for 24 h. The resulting crystalline material is a combination of hexanuclear Zr oxo-hydroxo clusters and the organic aromatic linker. The crystalline material had a topology of very high surface area and with unprecedented stability. In the present study, three different benzenedicarboxylic acids based linkers were examined for their ability to modify UiO-66 and generate the new, tagged MOF systems. The linkers studied included 2-amino-benzenedicarboxylic acid (NH_2-H_2BDC), 2-nitro-benzenedicarboxylic acid (NO_2-H_2BDC), and 2-bromo-benzenedicarboxylic acid ($Br-H_2BDC$), see Scheme 1.

The synthesis procedure adopted for the new, tagged MOFs slightly differs with respect to the one previously reported for UiO-66,[49] as the temperature conditions originally adopted for UiO-66 (120 °C for 24 h) only resulted in an amorphous phase. For this reason, we report here a very promising alternative approach in which the synthesis temperature increases by design during the crystallization step from 80 °C (12 h) to 100 °C (24 h). In addition, the synthesis was successfully and reproducibly scaled up by approximately a factor of 25 as detailed in the Experimental Section. These MOFs are therefore available on a larger scale. The resulting powders exhibit different colors depending on the funtionalization present on the linker: UiO-66-NH_2 (**1**) is yellow, whereas UiO-66-NO_2 (**2**) and UiO-66-Br (**3**) are both white. Repeated attempts at obtaining single crystals with dimension appropriate for single-crystal X-ray crystallographic studies by varying synthesis parameters, such as time, temperature program, stoichiometry, and solvents, were unsuccessful. Thus, the bulk crystallinity of each tagged MOF was instead evaluated by powder X-ray diffraction (PXRD). The diffraction patterns obtained for the as-synthesized samples are reported in Figure 1 (top) and reveal that the materials are indeed crystalline. All 2θ peaks were consistent with the as-synthesized UiO-66 parent material,[17] which demonstrates that the tagged UiO-66-X MOFs ($X = NH_2$ (**1**), NO_2 (**2**) and Br (**3**)) are topologically equivalent with UiO-66, as depicted in Figure 2. The UiO-66 structure was solved on the basis of the powder XRD pattern; it consists of an inner $Zr_6O_4(OH)_4$ core in which the triangular faces of the Zr_6 octahedron are alternatively capped by μ_3-O and μ_3-OH groups. All the polyhedron edges are bridged by the carboxylates (μ_2-(CO_2)) originating from the dicarboxylic acids to form a $Zr_6O_4(OH)_4(CO_2)_{12}$ cluster. Consequently, each Zr atom is eight-coordinated with a square-antiprismatic coordination geometry with all ligands being bonded through oxygen atoms. One square face of the square antiprism is formed by oxygen atoms supplied by

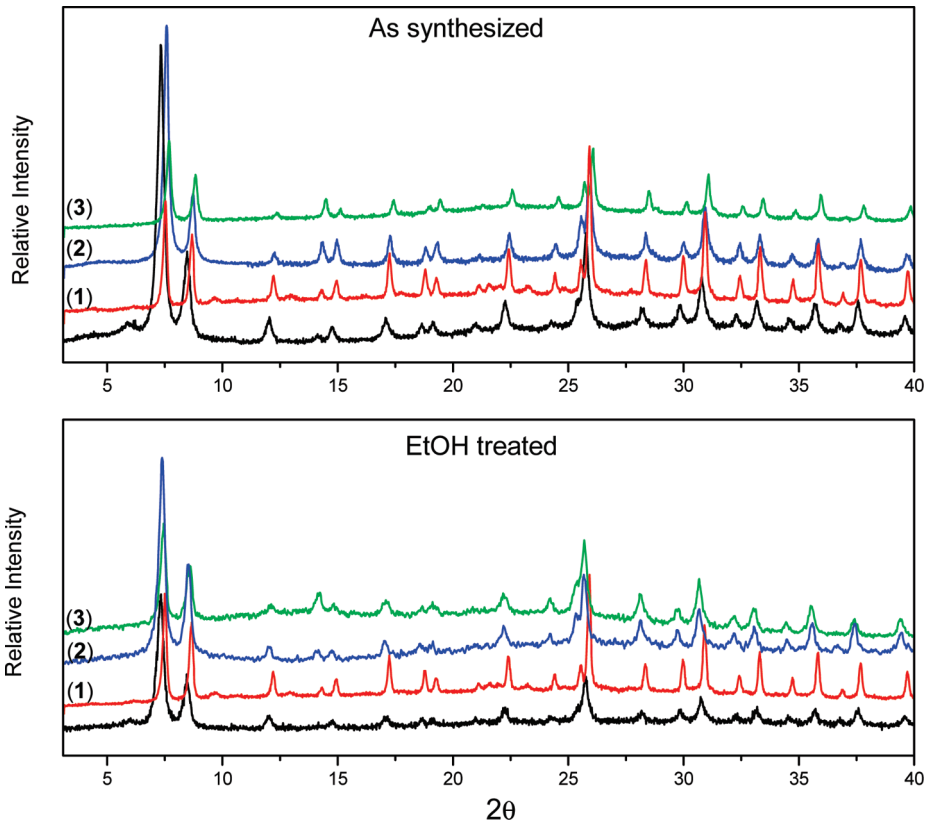

Figure 1. Comparison of PXRD patterns of UiO-66-NH_2 (**1**, red), UiO-66-NO_2 (**2**, blue), and UiO-66-Br (**3**, green) with untagged UiO-66 (black). Top: As-synthesized (from DMF) tagged MOFs. Bottom: Ethanol-exchanged tagged MOFs.

carboxylates, while the second square face is formed by oxygen atoms from the μ_3-O and μ_3-OH groups.[49]

One of the main properties of MOF materials is the presence of microporosity[50−54] that confers upon them interesting properties that are key to potential applications in different fields. In many instances, the high porosity (in the manifestation of inner surface physically available to external agents) can be obtained by thermal evacuation and by exchanging the solvent contained within the as-synthesized MOF with a lower boiling point solvent, followed by removal of the lower boiling solvent under relatively mild conditions. As reported by Nelson et al., solvent removal is usually a delicate operation that can lead to collapse or channel blockage.[55,56] In our case, a high-temperature thermal evacuation procedure is to a great extent hampered by the presence of the functional groups. Therefore, a liquid solvent exchange (e.g., DMF with ethanol) procedure was performed, followed by pore evacuation at moderate temperatures. PXRD measurements performed after exchange with ethanol (see Figure 1, bottom) demonstrated that the crystallinity was well preserved. However, a residual quantity of DMF was still present, as suggested by FTIR analysis (vide infra).

To evaluate the porosity, N_2 adsorption/desorption isotherms (see Supporting Information SI, Figure S1) were collected and the Langmuir surface areas were consequently calculated (Table 1). All isotherms of the crystalline tagged MOF samples were obtained at 77 K with N_2 and all were found to retain porosity despite the presence of different functional groups on the linker. The Langmuir surface area data were found to range from 1300 to 850 m^2/g. Observed decreases in surface area (~850 m^2/g for (**2**) and (**3**) vs ~1300 m^2/g UiO-66 and UiO-66-NH_2 (**1**)) are largely attributed to both reduced free space available and increased overall weight of the new MOF as a result of introducing large and heavy nitro groups and Br atoms.

IR and Raman Spectroscopy Characterizations. The presence of the introduced functional groups on the linkers was further evidenced by characterizing the MOFs under study with IR and Raman spectroscopies. The IR spectra were collected on samples prepared as thin films and the measurements were performed after solvent removal at 100 °C in vacuum. The Raman spectra were obtained on powder samples in air.

In Figure 3, the FTIR (left part) and Raman (right part) spectra of the tagged MOFs **1-3** are compared with the

(50) Devic, T.; Horcajada, P.; Serre, C.; Salles, F.; Maurin, G.; Moulin, B.; Heurtaux, D.; Clet, G.; Vimont, A.; Greneche, J. M.; Le Ouay, B.; Moreau, F.; Magnier, E.; Filinchuk, Y.; Marrot, J.; Lavalley, J. C.; Daturi, M.; Ferey, G. *J. Am. Chem. Soc.* **2010**, *132*, 1127–1136.
(51) Clegg, J. K.; Iremonger, S. S.; Hayter, M. J.; Southon, P. D.; Macquart, R. B.; Duriska, M. B.; Jensen, P.; Turner, P.; Jolliffe, K. A.; Kepert, C. J.; Meehan, G. V.; Lindoy, L. F. *Angew. Chem., Int. Ed.* **2010**, *49*, 1075–1078.
(52) Ma, L. Q.; Mihalcik, D. J.; Lin, W. B. *J. Am. Chem. Soc.* **2009**, *131*, 4610–4612.
(53) Lohe, M. R.; Rose, M.; Kaskel, S. *Chem. Commun.* **2009**, 6056–6058.
(54) Yaghi, O. M. *Nat. Mater.* **2007**, *6*, 92–93.
(55) Nelson, A. P.; Farha, O. K.; Mulfort, K. L.; Hupp, J. T. *J. Am. Chem. Soc.* **2009**, *131*, 458–460.
(56) Nelson, A. P.; Parrish, D. A.; Cambrea, L. R.; Baldwin, L. C.; Trivedi, N. J.; Mulfort, K. L.; Farha, O. K.; Hupp, J. T. *Cryst. Growth Des.* **2009**, *9*, 4588–4591.

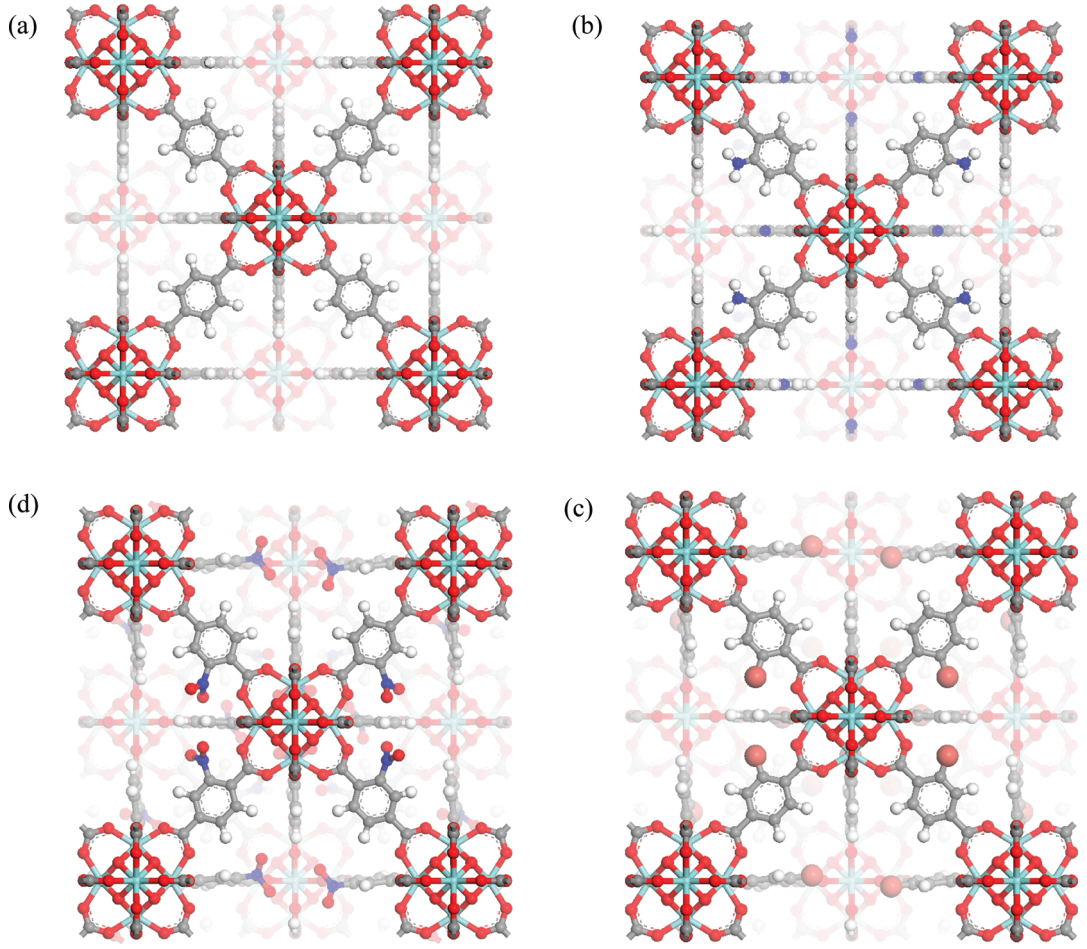

Figure 2. Depiction of Zr-MOFs with (a) 1,4-benzene-dicarboxylate (BDC) linker, UiO-66; (b) 2-amino-1,4-benzene-dicarboxylate (H_2N-BDC) linker, UiO-66-NH_2 (**1**); (c) 2-nitro-1,4-benzene-dicarboxylate (H_2N-BDC) linker, UiO-66-NO_2 (**2**); (d) 2-bromo-1,4-benzene-dicarboxylate (H_2N-BDC) linker, UiO-66-Br (**3**).

Table 1. Comparisons of Experimental Surface Areas (Langmuir) and Calculated[57] Surface Areas of UiO-66, UiO-66-NH_2 (1), UiO-66-NO_2 (2), and UiO-66-Br (3)

Langmuir surface area [m^2/g]	UiO-66	UiO-66-NH_2 (**1**)	UiO-66-NO_2 (**2**)	UiO-66-Br (**3**)
experimental	1300	1250	856	899
calculated	1187	996	839	817

spectra of the parent UiO-66. The FTIR spectrum of the amino-tagged sample UiO-66-NH_2 (**1**) is depicted in Figure 3, parts (a) and (b). Spectroscopic features due to the presence of the amino group can be discerned in the whole spectral region and in particular in the high frequency region where the primary aromatic amino group displays two medium absorptions, one at 3507 cm^{-1} and the other at 3384 cm^{-1}. These bands represent, respectively, the asymmetric and symmetric N−H stretching modes. Upon treatment with D_2O vapors, these bands underwent the expected isotopic shifts with new bands appearing at 2618 and 2478 cm^{-1} which are assigned to asymmetric and symmetric N-D stretching modes, respectively (see SI, Figure S2). Importantly, this H/D scrambling shows that the amino group is accessible as well as chemically reactive. An analysis of the lower frequency region of the IR spectra requires particular attention due to the presence of a great number of bands, partially discussed and analyzed in our previous report,[49] and the bands are largely assigned to skeletal vibration modes of the material (combination of modes due to the organic aromatic linker and the Zr cluster unit). Among these features, it is possible to distinguish two other characteristic bands of the amino group: the medium N−H bending (scissoring) vibration observed at 1626 cm^{-1} and the strong C−N stretching absorption distinctive of aromatic amines at 1356 cm^{-1}. This assignment has been further confirmed by recording the IR spectrum of the linker (NH_2−H_2BDC) (see SI, Figure S3). The spectroscopic features of the linker amino group are seen and compared with the ones observed for UiO-66-NH_2. There is evidently a good match between bands assigned to the -NH_2 functionalization ($\nu_{asym}(-NH_2)$, $\nu_{sym}(-NH_2)$, $\delta(-NH_2)$, and ν(C−N)). Unfortunately, the Raman spectrum of UiO-66-NH_2 (**1**) is not available as this material is fluorescent and the detection of its typical spectroscopic features is not possible.

Parts c and d in Figure 3 report the FTIR spectrum of UiO-66-NO_2. The presence of the nitro group at the linker is confirmed by the presence of typical spectroscopic features arising from aromatic nitro compounds. In particular, the nitro group shows absorption because of asymmetric (ν $(NO)_{asym}$) and symmetric ($\nu(NO)_{sym}$) stretching modes. Asymmetric modes typically result in a strong

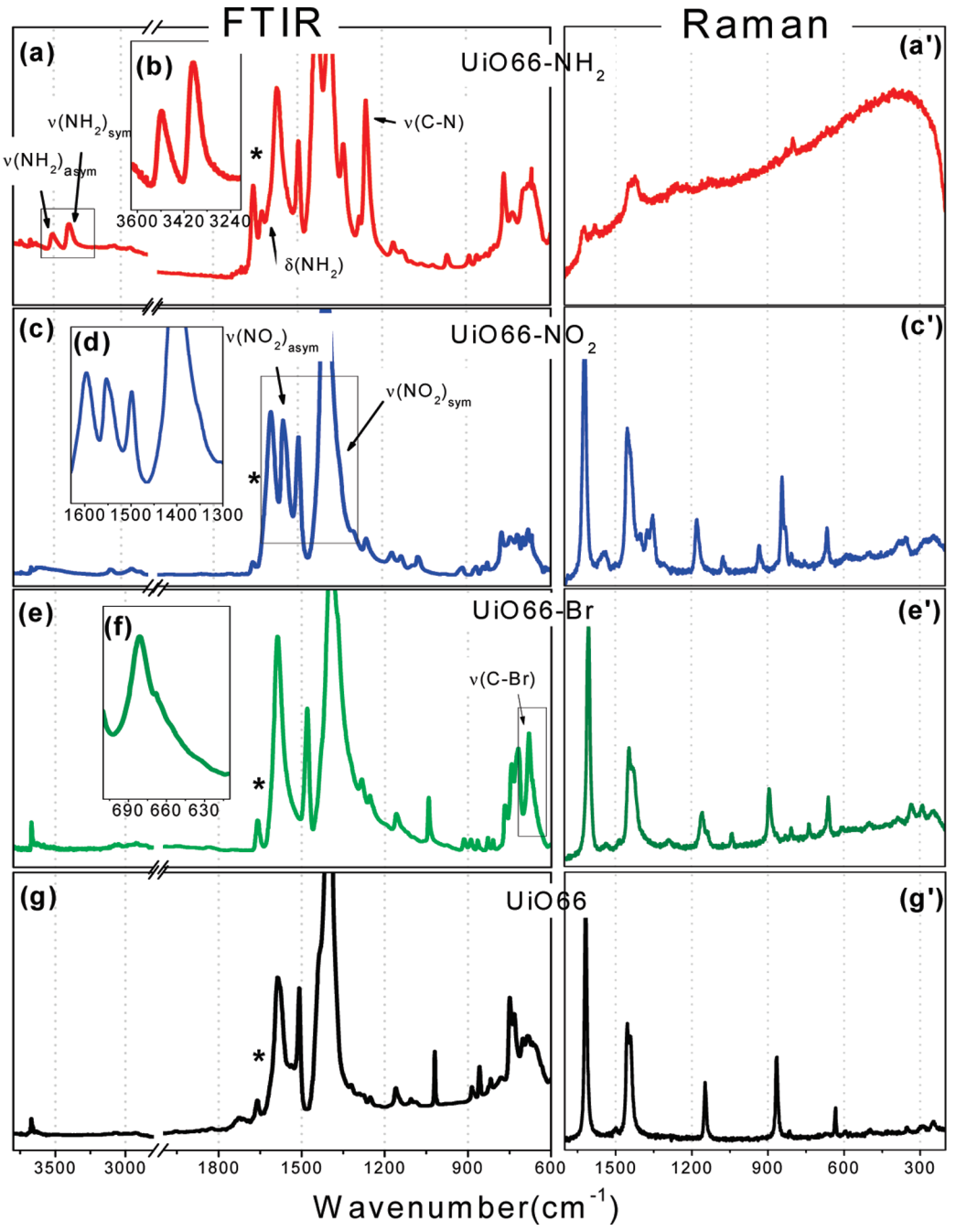

Figure 3. Left part: FTIR spectra of tagged Zr-MOFs activated at 373 K in vacuum. (a) UiO-66-NH_2 (**1**); (b) magnification of the of the $\nu(NH_2)_{asym}$ and $\nu(NH_2)_{sym}$ region; (c) UiO-66-NO_2 (**2**), (d) magnification of the of the $\nu(NO_2)_{asym}$ and $\nu(NO_2)_{sym}$ region; (e) UiO-66-Br (**3**); (f) magnification of the ν(C−Br) region; (g) UiO-66. Vibrational modes due to the presence of functional groups are indicated. * denotes residual DMF. Right part: Raman spectra of tagged Zr-MOFs recorded in air. (a′) UiO-66-NH_2 (**1**); (c′) UiO-66-NO_2 (**2**); (e′) UiO-66-Br (**3**); (g′) UiO-66.

band in the 1550−1500 cm^{-1} region; symmetric modes absorb in the 1360−1290 cm^{-1} region. In our case, UiO-66-NO_2 (**2**) shows, when compared with UiO-66 (Figure 3g), the presence of two additional bands in the above-mentioned regions. The first is centered at 1554 cm^{-1} and the second, partially overshadowed by a strong band attributed to a carboxylate mode, appears as a shoulder at approximately 1355 cm^{-1}. These bands can be reasonably ascribed to the NO_2 group. As expected, similar absorptions were observed also in the IR spectrum of the NO_2−H_2BDC linker (see SI, Figure S3), further validating the assignment. The C−N stretching vibration ν(C−N) usually present in nitroaromatic compounds near 870 cm^{-1} is not straightforwardly assigned.[58] The Raman spectrum (c′), which in this case can be obtained because the sample does not fluoresce, exhibits many features in the 1700−200 cm^{-1} range. These mostly resemble the typical Raman bands of parent UiO-66 shown in Figure 3, part (g′), except for some minor shifts in some cases.[59] Here, bands ascribed to benzene ring and

(57) Duren, T.; Millange, F.; Ferey, G.; Walton, K. S.; Snurr, R. Q. *J. Phys. Chem. C* **2007**, *111*, 15350–15356.

(58) Socrates, G. *J. Chem. Educ.* **1995**, *72*, A93.

(59) Valenzano, L.; Civalleri, B.; Chavan, S.; Bordiga, S.; Nilsen, M. H.; Jakobsen, S.; Lillerud, K. P.; Lamberti, C. Chem. Mater. In press.

carboxylate vibrational modes are readily distinguished, while the vibrational features involving the Zr-containing moiety are hardly detected. However, in UiO-66-NO_2 (**2**) some differences can be appreciated. The most prominent is the new band centered at 1360 cm^{-1} ascribable to $\nu(NO_2)_{sym}$.[60] Furthermore, other new bands appear in the 1100−900 cm^{-1} range and at the lowest frequencies. The FTIR spectrum recorded for UiO-66-Br (**3**) shows (Figure 3, parts (e) and (f)) a profile that is quite similar to the one obtained for UiO-66 (Figure 3, part (g)). Although there are no pure carbon−halogen stretching vibration modes for aromatic halogen compounds,[61] the presence of peaks sensitive to the bromo functionality are evidenced. In particular, the main bands involving the carbon−bromine bond vibration were seen at 680 cm^{-1}; a similar band was seen for the Br-H_2BDC linker (see SI, Figure S3).[62] The Raman spectrum of UiO-66-Br (**3**) reported in Figure 3, part (e′), presents again common features also seen for UiO-66 in Figure 3, part (g′), except of course for some small band shifts. As previously observed, some new bands (1040, 736, 290 cm^{-1}) that are not straightforwardly assigned also appear. In this case, the assignment of vibrational modes involving Br is more difficult.

Preliminary experiments performed following CO_2 adsorption with FTIR spectroscopy show an equivalent response (see SI, Figure S4) testifying to a similar behavior of the tagged materials and the pristine UiO-66 with respect to CO_2 adsorption.

Thermal Stability of Tagged MOFs. To confirm the stability and structural integrity of **1**−**3** at elevated temperatures, samples of each were examined by TGA. The ethanol-treated samples were first dried under vacuum to remove any residual solvent. All the tagged samples exhibited different thermal stabilities compared to that of UiO-66 with observed decomposition temperatures between 350 and 500 °C in air (Figure 4). An interesting question that arises at this point is: Which functional group properties will affect MOF decomposition temperatures? First, if we consider electronic effects, the NH_2-tagged MOF (**1**) is electron rich and the NO_2-tagged MOF (**2**) is electron poor, based on the Hammett σ values for these substituents.[63] Yet, these MOFs undergo decomposition at rather similar temperature at ∼350 °C, whereas the Br-tagged MOF (**3**) and the parent ("H-tagged") MOF (UiO-66) which have Hammett σ values somewhere in-between, decompose at considerably higher temperatures, ∼500 °C. Next, if we consider steric effects alone, the sterically hindered UiO-66-Br (**3**) decomposes at a similar temperature as the least hindered UiO-66, ∼500 °C. By comparison, UiO-66-NH_2 (**1**) of intermediate steric hindrance and UiO-66-NO_2 (**2**), of similar steric hindrance as UiO-66-Br (by simple inspection of Chem3D spacefilling models of the respective X-substituted benzenes) undergo decomposition at the considerably lower temperatures at ∼350 °C. Thus,

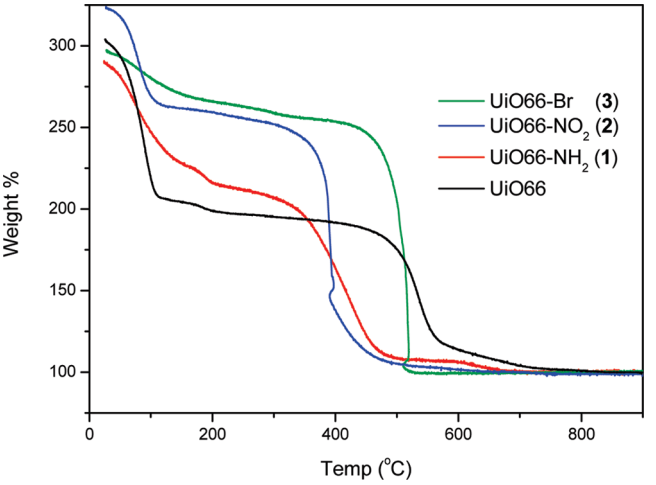

Figure 4. TGA analysis of UiO-66 (black), UiO-66-NH_2 (**1**, red), UiO-66-NO_2 (**2**, blue), and UiO-66-Br (**3**, green). Weight % is relative to high-temperature residue (ZrO_2 by PXRD).

neither electronic nor steric requirements of the functional groups in the molecular linkers appear to offer simple correlations with the observed thermal stability, and thus the origin of the differences is as yet unclear. However, these variations notwithstanding, it is important to note that all these tagged MOFs have exceptionally high thermal stabilities.

The decomposition during a TGA experiment was also monitored by mass spectrometry for UiO-66 and UiO-66-NH_2 (**1**) (see SI, Figure S5). At the temperature of lattice breakdown (T_{decomp} = 540 °C for UiO-66 and 350 °C for UiO-66-NH_2), benzene and CO_2 fragments were observed in the gas phase by MS, suggest the breakdown of the connection between the linker and the inorganic brick and also of the bond between the benzene rings and the terminal carboxyl group. It is not clear whether these fragments are primary or secondary decomposition products and thus it remains unclear whether cleavage of the benzene-carboxylate group is a crucial step in the thermal breakdown.

Temperature-Resolved XRD. The thermal stabilities and decompositions of the tagged materials were also monitored by temperature-resolved powder XRD, as shown in Figure 5. UiO-66-NH_2 (**1**) and UiO-66-NO_2 (**2**) (Figure 5a and b) exhibited quite similar decomposition behavior. Initially, the materials were well crystalline with the UiO-66 topology. From 100 to 250 °C, a slight increase in intensity of the (111) reflection ($2\theta = 7.283°$) was observed, which is due to the removal of the solvent (DMF). For UiO-66-NH_2 (**1**), another effect of the solvent removal is the disappearance of the two peaks at 2θ lower than the (111) reflection, which represents forbidden reflections for the topological space group ($Fm\bar{3}m$ (225)), but these broad peaks index in the right cubic cell if the symmetry is reduced to primitive. A decrease in the intensities at around 300 °C was observed for both materials (290 °C for UiO-66-NH_2 (**1**) and 310 °C for UiO-66-NO_2 (**2**)), followed by a peak broadening clearly showing the decomposition of the material. At 410 °C, UiO-66-NH_2 (**1**) and UiO-66-NO_2 (**2**) were fully decomposed. These results are in accordance with the TGA analyses (Figure 4), where the decompositions started

(60) Clarkson, J.; Smith, W. E. *J. Mol. Struct.* **2003**, *655*, 413–422.
(61) Socrates, G. *J. Am. Chem. Soc.* **2001**, *124*, 1830–1830.
(62) Bertie, J. E.; Sunder, S. *Can. J. Chem.* **1973**, *51*, 3344–3353.
(63) Hansch, C.; Leo, A.; Taft, R. W. *Chem. Rev.* **1991**, *91*, 165–195.

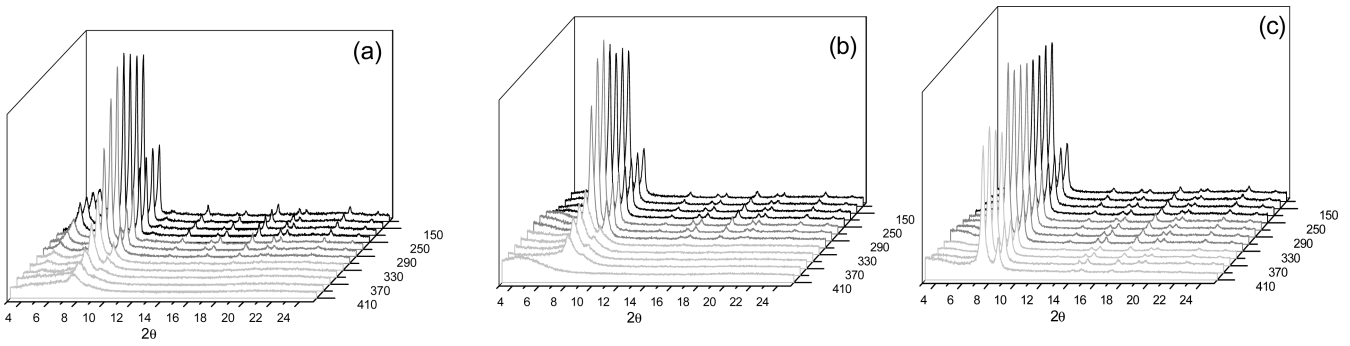

Figure 5. Thermal stabilities of the three tagged UiO-66 materials monitored by temperature-dependent powder XRD: (a) UiO-66-NH_2 (**1**); (b) UiO-66-NO_2 (**2**); (c) UiO-66-Br (**3**). The two temperature intervals studied are 100−250 °C (increments of 50 °C) and 250−410 °C (increments of 20 °C). Note that the temperature is increasing from back to front.

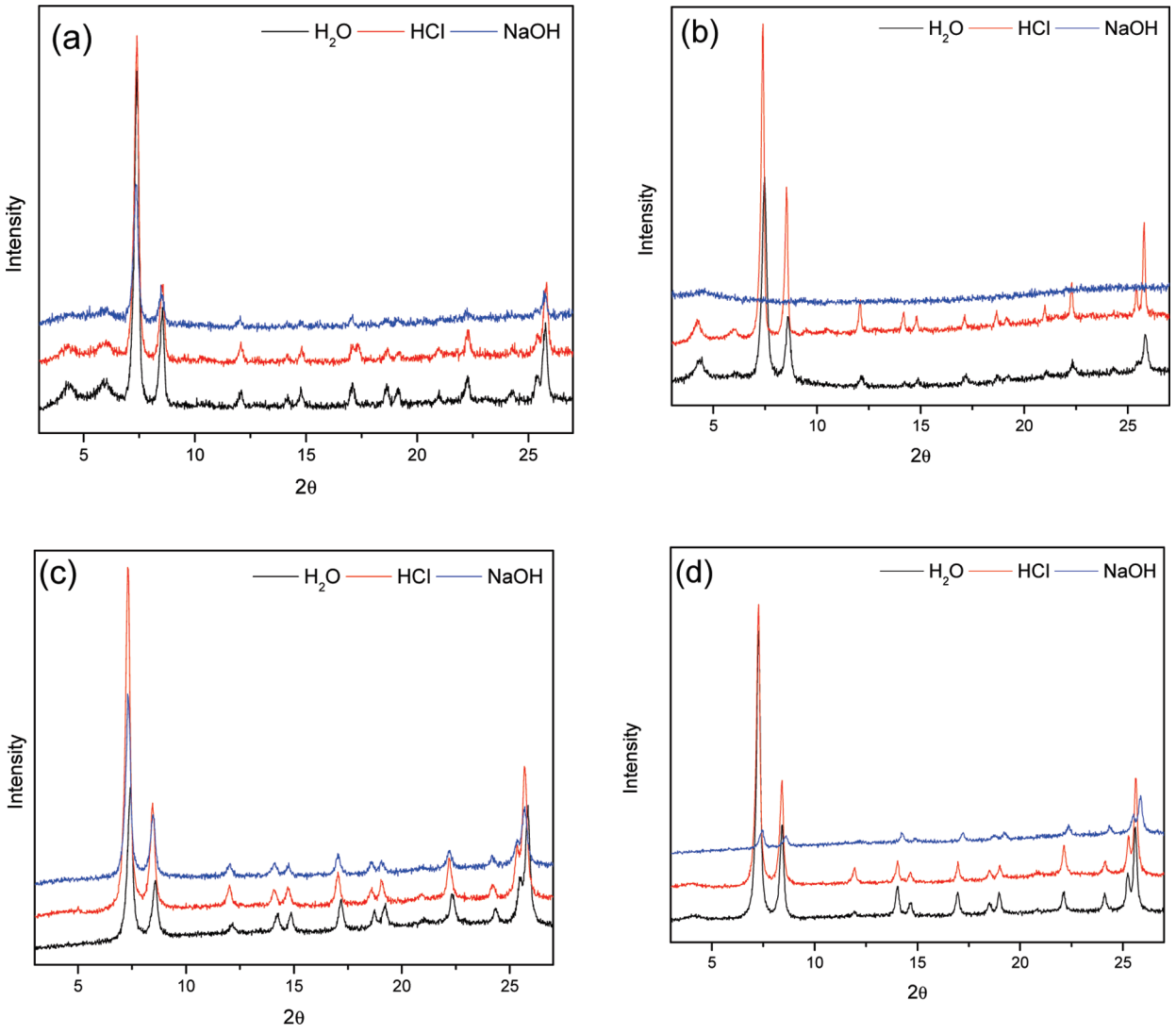

Figure 6. Powder X-ray diffractograms of the tagged UiO-66 materials showing the stability toward treatment with H_2O, HCl (pH = 1), and NaOH (pH = 14). (a) for comparison, UiO-66; (b) UiO-66-NH_2 (**1**); (c) UiO-66-NO_2 (**2**); (d) UiO-66-Br (**3**). See also Figure 1 for the as-synthesized PXRDs.

at around 300 °C, albeit at a somewhat lower temperature for UiO-66-NH_2 (**1**) than for UiO-66-NO_2 (**2**). The temperature-resolved PXRD for UiO-66-Br (**3**) (Figure 5 c) demonstrated a higher thermal stability for this material compared to UiO-66-NH_2 (**1**) and UiO-66-NO_2 (**2**). Although a decrease in signal intensities was observed, no peak broadening could be seen in the temperature range studied. This confirms the TGA results in that UiO-66-Br (**3**) starts to decompose at ca. 450 °C.

Stability towards Chemical Treatment. The stabilities of UiO-66 and the tagged materials **1**−**3** towards water, acid (HCl, pH = 1) and base (NaOH, pH = 14) were qualitatively studied and characterized by PXRD (Figure 6). UiO-66 samples were immersed in the desired solvent for 2 h at room

temperature. In general, the results showed that these materials, in addition to exhibiting exceptionally high thermal stabilities, also revealed quite high resistance toward these chemical treatments, similar to or better than the parent, untagged UiO-66 MOF. PXRD patterns collected for each sample showed that they maintain their full crystallinity in water and HCl. However, only UiO-66-NO_2 (**2**) (Figure 6c) retained its crystalline structure in NaOH, whereas UiO-66 (Figure 6a) and UiO-66-Br (**3**) (Figure 6d) were transformed to less crystalline materials within 2 h. We note that the most pronounced exception is the treatment of UiO-66-NH_2 (**1**) with NaOH, which led to a total decomposition of the MOF, in that an amorphous phase was indicated by PXRD (Figure 6b).

The exceptional robustness of UiO-66 and most of its functionalized derivatives toward aqueous and acidic conditions is promising inasmuch as new perspectives open up for the future application of these materials. Evidently, the connection between the hexanuclear Zr cluster cornerstones and the dicarboxylate linkers in UiO-66 and **1**−**3** is quite resistant toward hydrolysis, in particular in neutral and acidic media and this inhibits dissolution of the frameworks in aqueous HCl. In contrast, aqueous NaOH does degrade the functionalized MOFs, in particular UiO-66-NH_2. As we have discussed already, at this time we cannot straightforwardly identify which functional group properties are responsible for MOF thermal stability. The same pertains to which functional properties are responsible for differences in chemical stability of these tagged MOFs as well.

Conclusions

A family of isoreticular MOFs, based on the parent UiO-66 MOF, was obtained from the three different linker ligands 2-amino-benzenedicarboxylic acid (H_2N-H_2BDC), 2-nitro-benzenedicarboxylic acid (O_2N-H_2BDC), and 2-bromo-benzenedicarboxylic acid ($Br-H_2BDC$). The physicochemical and chemical investigation of these materials demonstrate that this class of MOFs retain high thermal and chemical stabilities, even with functional groups present at the linker units. It is not clear what factors contribute to the observed differences in thermal or chemical stabilities.

The results demonstrate the possibility of incorporating active functional groups into the UiO-66 structure almost without losing its exceptionally high thermal and chemical stability. It has been established that the functional groups, at least in the amino functionalized UiO-66 sample, are chemically available as evidenced by the H/D exchange experiment, making the tagged UiO series MOFs very interesting for further studies within the field of catalysis. Postsynthetic modifications of the MOFs are currently under investigation in our laboratories. Ongoing experimental efforts as well as future efforts planned for exploring the stabilities and other properties of these MOFs by computational methods will hopefully shed some more light on these issues and guide the further development of these materials for use in catalysis and other areas.

Acknowledgment. The authors thank Dr. Sachin Chavan for CO_2 adsorption measurements at the University of Torino and the Research Council of Norway (project no. 143143 to M.K. and project no. 182544 to S.U.), VISTA (project no. 6457 to M.H.N.) and the STREP project MOFCAT (Contract No. NMP4-CT-2006-033335 E.A.Q. and C.L.) for financial support.

Supporting Information Available: FT-IR characterization (D_2O exchange, linker analysis and CO_2 adsorption) and surface area isotherms. This material is available free of charge via the Internet at http://pubs.acs.org.